Effect of the Ni-doping on the vortex pinning of $CaK(Fe_{1-x}Ni_x)_4As_4$ single crystals

N. Haberkorn,[1,2] M. Xu,[1,3] W. R. Meier,[1,3] J. Schmidt,[1,4] S. L Bud'ko,[1,3] P. C. Canfield.[1,3]

[1] Ames Laboratory, US DOE, Iowa State University, Ames, Iowa 50011, USA.

[2] Centro Atómico Bariloche and Instituto Balseiro, CNEA and Consejo de Investigaciones Científicas y Técnicas Av. E. Bustillo 9500, R8402AGP, S. C. Bariloche, RN, Argentina.

[3] Department of Physics and Astronomy, Iowa State University, Ames, Iowa 50011, USA.

[4] Departamento de Física, FCEyN, and IFIBA-CONICET, Universidad de Buenos Aires, Buenos Aires 1428, Argentina.

.

Abstract

We study the correlation between chemical composition and vortex dynamics in Ni-doped $CaK(Fe_{1-x}Ni_x)_4As_4$ (x = 0, 0.015, 0.025, 0.03 and 0.05) single crystals by performing measurements of the critical current densities J_c and the flux creep rates S. The magnetic relaxation of all the crystals is well described by the collective creep theory. The samples display a glassy exponent, μ, within the predictions for vortex bundles in a weak pinning scenario and relatively small characteristic pinning energy (U_0 < 100 K). The undoped crystals display modest J_c values at low temperatures and high magnetic fields applied along the c-axis. $J_c(T)$ dependences at high fields display an unusual peak. The enhancement in $J_c(T)$ matches with an increase in U_0 and the appearance of a second peak in the magnetization (SPM). As Ni doping increases whereas there is a monotonic decrease in T_c there is a non-monotonic change in J_c. Initially J_c increases, reaching a maximum value for x = 0.015, and then J_c decreases for x ≥ 0.025. This change in $J_c(x)$ is coincident with the onset of antiferromagnetic order. The magnetic field dependence of $J_c(H)$ also manifests a change in behavior between these x-values. The analysis of the vortex dynamics for small and intermediate magnetic fields shows a gradual evolution in the glassy exponent μ with Ni-content, x. This implies that there is no appreciable change in the mechanism that determines the vortex relaxation.

Keywords: iron based superconductors; vortex dynamics; critical current densities.

1. Introduction

The critical current densities J_c in type II superconductors depend on a complex interplay of individual pinning centers, the interaction between vortices, and the thermal fluctuations [1,2]. The discovery of iron-based superconductors (Fe-SCs) allowed for an expansion of the knowledge about the influence of intrinsic superconductor parameters on the resulting vortex dynamics [3,4]. The different families of Fe-SCs display superconducting transition temperatures T_c up to 56 K [5,6,7]. These materials usually exhibit strong interplay between superconductivity and magnetism [8]. The electronic properties depend on doping (substitutional disorder) and are also affected by pressure [5,6,7,9,10,11]. Vortex dynamics in Fe-SCs is usually well described by the collective creep theory [12,13,14]. The sources of flux pinning include random point defects [15], precipitates [16], planar defects [17] and correlated disorder such as twin boundaries [18]. Notwithstanding the coexistence between superconductivity and magnetism usually present in many Fe-SCs [19,20,21], its influence on the resulting vortex dynamics has been little explored.

The current carrying capacity is a relevant parameter which determines the range of applications of new superconducting materials. Single crystals are the starting point to evaluate the vortex pinning mechanisms. The temperature T and magnetic field H dependences of J_c in any superconductor depend on the type and density of pinning centers. The J_c (H) dependences in Fe-SCs usually display several regimes as a consequence of a pinning landscape with random point disorder and a low-density of large defects [15]. Depending on the disorder at the nanoscale, the J_c (H) curves may decrease monotonically or display a second peak in the magnetization (SPM) or fishtail [12,13,14]. On the other hand, because of thermally activated vortex motion, J_c data usually decrease with temperature. An exception to that has been recently observed in $CaKFe_4As_4$ single crystals [16,17,22,23]. For instance, as a consequence of smoother J_c (H) dependences, the J_c value for $\mu_0 H$ = 5 T at 20 K is higher than that observed at 10 K. This unusual behavior has been related to the presence of planar $CaFe_2As_2$ intergrowths [16].

$CaKFe_4As_4$ is a member of the so-called 1144 family $AeAFe_4As_4$ (Ae = Ca, Sr, Eu and A = K, Rb, Cs). $CaKFe_4As_4$ has a tetragonal structure (P4/mmm), where Ca and K layers stack alternatively across the Fe_2As_2 layer along the c axis [24]. The undoped compound is a multiband superconductor with $T_c \approx 35$ K with no other identified phase transition (magnetic or

structural) [24,25,26]. Under pressure, T_c is suppressed and then superconductivity disappears at $p \geq 4$ GPa due to a structural phase transition into a half collapsed tetragonal state [27]. The extrapolated upper critical field at zero temperature for $CaKFe_4As_4$ is ≈ 70 T with a coherence length ξ_{GL} (0) ≈ 1.4 nm [25]. The anisotropy parameter $\gamma = {H_{c2}^{\perp c}}/{H_{c2}^{//c}}$ for **H** applied perpendicular and parallel to the *c* axis increases with the temperature being 1.5 at 25 K and 2.5 near T_c [26]. The penetration depth estimated using muon-spin rotation is λ(0) = 208 (4) nm [28]. Although no substitutional disorder is expected, low-temperature scanning tunneling microscope (LT-STM) data reveal the presence of locations with suppression of the superconducting order parameter [29]. Gradual suppression of the T_c and the emergence of magnetic order take places via Co or Ni substitution onto the Fe site [30,31]. As shown in Fig. 1*b*, coexistence of superconductivity and antiferromagnetism (AFM) appears for adequate doping [21]. Moreover, the Ni/Co addition should modify the vortex pinning landscape by introducing disorder due to chemical substitution.

In this work, we analyze the influence of the Ni doping on the vortex dynamics of $CaK(Fe_{1-x}Ni_x)_4As_4$ single crystals (x = 0, 0.015, 0.025, 0.03 and 0.05) by performing magnetization measurements. We systematically study the influence of the Ni addition on the J_c (T, H) dependences. The vortex dynamics are analyzed in the framework of the collective creep theory [32]. We measure the flux creep rate $S = -{\delta lnJ}/{\delta lnt}$ as a function of the temperature and the magnetic field. The effective barrier height for flux creep rates and glassy exponent μ are analyzed by the extended Maley method [33].

2. Experimental

Single crystals of Ni-doped $CaKFe_4As_4$ were grown out of a high-temperature solution rich in transition-metals and arsenic similar to the procedure used for the pure compound [26,30,34]. The study is performed using $CaK(Fe_{1-x}Ni_x)_4As_4$ single crystals with T_c = 35 K (x= 0), 31.1 K (x= 0.015), 25 K (x= 0.025), 20.5 K (x= 0.03) and 10.1 K (x= 0.05). The single crystals exhibit a plate-like morphology with the *c* axis perpendicular to the plane of the plate. The samples used were roughly rectangular plates with length *l,* width, w, and thickness *d*. The magnetization (**M**) measurements were performed using a superconducting quantum interference device (SQUID)

magnetometer. The thicknesses *d* were calculated using the area (l × *w*), the superconductor volume and the Meissner slopes with **H**||ab considering the proper demagnetization factor. The volume and the mass of all the single studied crystals agree with the density determined from lattice parameters, 5.22 g/cm^3 [24]. The J_c values were calculated from the magnetization data using the appropriate geometrical factor in the Bean Model [35,36]. For **H**||*c*, $J_c = \frac{20\Delta M}{w(1 - w/(3l))}$, where Δ*M* is the difference in magnetization *M* (emu/cm^3) between the top and bottom branches of the hysteresis loop. The creep measurements, *M*(*t*), were recorded over a time above 60 minutes. The magnetization of the sample holder was measured and subtracted from the data by averaging the initial points of the time relaxation for the lower and upper magnetic branches. The initial time was adjusted considering the best correlation factor in the slope of $S = -{}^{\delta lnJ}/_{\delta lnt}$. The initial critical state for each creep measurement was generated using $\Delta H \sim 4\ H^p$, where H^p is the field for full flux penetration estimated as $H^p = {}^{J_c d}/_2$ [37].

3. Results and discussion

Figure 1*a* shows the temperature dependence of the normalized magnetization (M (T) /M (5 K)) for the studied single crystals. The measurements were performed with **H** // *c*- axis under zero-field cooling (ZFC) with an applied magnetic field of 0.5 mT. The T_c value decreases systematically from 35 K for the undoped single crystal to ≈ 10.1 K for $CaK(Fe_{0.95}Ni_{0.05})_4As_4$ (see Table I). Figure 1*b* shows a schematic *x*-*T* phase diagram for $CaK(Fe_{1-x}Ni_x)_4As_4$ and the corresponding position of the studied samples [30]. The single crystals with x > 0.02 display coexistence of superconductivity and AFM order [21,30,31].

Figure 2 shows the J_c (*H*) dependences at different temperatures for each chemical composition obtained from hysteresis loops (see Appendix). The curves are plotted on log-log scales. Partial data at 1.8 K are shown due to flux jumps. The J_c (*H*) dependences display a low field saturation followed by a power-law regime, followed by a local maximum associated with a second peak in the magnetization (SPM). The latter becomes very weak in x =0.05. The power-law is related to a low density of strong pinning centers and the SPM to random point disorder [15]. The (J_c/J_0) ratio is a parameter that determines the strength of the pinning potential (with $J_0 = cH_c / 3\sqrt{6}\pi\lambda$

≈ 170 MA cm^{-2}, H_c the thermodynamic critical field and c the speed of light) [32]. The undoped crystal displays self-field J_c^{sf} (1.8 K) ≈ 2.4 MA.cm^{-2} and (J_c/J_0) ≈ 0.014. The low fraction of J_0 is similar to that found in single crystals of other Fe-SCs [38,39]. Depending on the magnetic field strength, several regimes of the J_c (H) behavior are observed (see Fig. 2*b*): a low-field regime ($B<B^*$) that could be associated with the single vortex regime (SVR) but that is also strongly affected by the self-field; (II) a power-law dependence $J_c \propto H^{-\alpha}$ related to strong pinning centers; (III) a third regime (at the end of the power-law) related to random disorder with $J_c(H) \approx$ constant or a SPM; and (IV) a high-field regime which is characterized by a fast drop in J_c (H) and is usually related to a crossover from elastic to plastic relaxation of the vortex lattice [12]. As is usual, if the temperature increases, the in-field position at the maximum of the SPM decreases.

At first glance, there is a qualitative difference between the undoped and the doped samples related to regime III. The undoped crystals display an unusual maximum at J_c (T) at intermediate temperatures (see Fig. 2a) [16,17,22,23]. The effect disappears for Ni-doped samples. In fact, the J_c (H) curves are similar to those reported in other systems such as Co-doped $BaFe_2As_2$ [40,41] and $Ba_{1-x}K_xFe_2As_2$ [42,43]. However, unlike these Fe-SCs, the pinning in $CaK(Fe_{1-x}Ni_x)_4As_4$ cannot be related to orthorhombic structural domains [40,42]. Figure 2*f* (left axis) shows a summary of J_c^{sf} and J_c^{4T} at 5 K. Although the data correspond to different T/T_c values, it is useful to analyze the influence of the Ni-addition on the J_c values at low and high magnetic fields. The results show that small Ni addition improves J_c in the whole range of magnetic fields, indicating that the disorder produced by chemical inhomogeneities enhances vortex pinning. The $J_c^{sf}(x)$ displays a maximum value of 2.8 MA cm^{-2} at x = 0.015 that systematically drops at larger doping. To rule out any effect related to the thickness (d) in the J_c^{sf} enhancement, we also measure a thinner undoped crystal (see Table I) [44]. Although J_c^{sf} increases from 1.7 MA.cm^{-2} (d = 34 μm) to 2.0 MA.cm^{-2} (d = 14 μm), its qualitative x dependence is unaffected.

It should be noted that both $J_c(x)$ and α (x) data (shown in Figure 2*f*) show a clear change in behavior between x = 0.015 and x = 0.025, i.e. a clear change in behavior as the sample develops an AFM ordered ground state that coexists with a competing superconducting state. J_c(x) for self-field shows a discontinuous break with a clear maximum on the low-x side (x = 0.015). J_c(x) for $\mu_0 H$ = 4 T also has a maximum value for x = 0.015. Whereas similar behavior was found for Co-doped $BaFe_2As_2$, [40] in the case of Ni-doped $CaKFe_4As_4$ structural domains associated with a low temperature, orthorhombic structure are absent. If indeed the local

maximum in J_c is associated with onset of hedgehog-spin vortex crystal AFM order [30,31], then this implies that AFM domains, not structural ones, are playing a key role. This change in pinning may also be responsible for the more gradual decrease in α in the antiferromagnetic state. The J_c^{4T} (x) curve shows a broad maximum spanning from $x \approx 0.015$ to 0.03. The $J_c^{4T}(5\ K) \approx 0.27$ MA cm^{-2} observed for the undoped crystal increases to 0.7-0.5 MA cm^{-2} for x = 0.015-0.03. The influence of the Ni-addition on the pinning at high magnetic fields is also evident from the reduction of the $J_c^{sf}/\ J_c^{4T}$ ratio. The analysis of the different vortex pinning regimes as a function of Ni doping is presented below.

The regimes (I) and (II) have been described by strong pinning produced by normal inclusions [15]. The regime (I) corresponds to the SVR and is limited by vortex-vortex interactions at B^* (see Fig. 2*b*). However, experimentally the single-vortex pinning is overlapped by self-field effects ($B^* \approx J_c$ x *thickness*) making its analysis difficult [45]. In addition to the changes in the absolute J_c values, the additional disorder at the nanoscale, produced by Ni substitution modifies the power-law dependence $J_c \propto H^{-\alpha}$. The α values decrease systematically from ≈ 0.68 to ≈ 0.40 as the Ni-doping increases (see right axis in Fig. 2*f* and Table I). As we mentioned above, the α values go towards values smaller than 0.5 changing more gradually when AFM and superconductivity coexist. A gradual reduction in the α value is usually observed in superconductors as the disorder in the nanoscale increase by adding random point defects [4646]. It is important to note that, although there is a peak in $J_c(T)$ at high magnetic fields, the α values in the undoped crystals remain ≈ constant increasing temperature. To understand the origin of the pinning in the undoped sample is necessary to consider LT-STM data [29]. The vortex pinning to magnetic fields up 8 T at 0.8 K is produced by defects with a size comparable to ξ. From a geometrical point of view, the crossover from strong to weak pinning occurs when $\sqrt{2}\xi(T) > r_d$ (with r_d the radius of the defect) [32]. Moreover, the pinning can be affected by a reduction in the ξ value when the magnetic field is increased [29].

The $J_c(H)$ dependence at the power-law produced by a random distribution of nanoparticles has been theoretically predicted as [47]:

$$J_c \approx 0.0866 n_i J_0 \frac{[DF(T)]^{9/4}}{\varepsilon \xi^{1/2}} \left(\frac{\Phi_0}{H}\right)^{5/8}, \qquad (1)$$

where n_i is the density of the pinning particles, D is their diameter (assuming that they are spherical), ε the anisotropy parameter and $F(T) \approx \ln\left[1 + D^2/8\xi^2(T)\right]$. Although for the undoped sample α is slightly larger than 5/8, it is useful to compare the absolute J_c values at low temperatures with expected density of strong pinning centers. Using $\xi \approx 1.4$ nm and $D = 3$-4 nm, we obtain $F(0) \approx 0.45 - 0.7$. The $J_c(H)$ average values at 1.8 K (i.e. 1.7 MA.cm^{-2} at 0.7 T and 0.43 MA.cm^{-2} at 4.5 T) with $J_0 = 170$ MA cm^{-2}, corresponds to $n_i \approx 1\text{x}10^{17}$ cm^{-3} - $5\text{x}10^{17}$ cm^{-3}. These values indicate defects at distances of ≈ 15 - 25 nm, which is in agreement with LT-STM data where a disordered vortex lattice is observed to magnetic fields up 8 T at 0.8 K (inter-vortex distance ≈ 18 nm) [29]. A similar analysis may be performed in Ni-doped samples. The differences in the absolute values of J_c are produced by both changes in the superconducting parameters (such as ξ and λ), and variations in the density and size of the crystalline defects.

Regime III should be analyzed considering vortex pinning produced by random disorder ($\sqrt{2}\xi(T) > r_d$) [32]. As we mentioned earlier, the undoped crystal displays modest J_c values at low temperatures and high magnetic fields. Moreover, $J_c(H) \approx$ constant is expected for temperatures below 20 K [23]. The simplest possibility is that regimes I and II are due to a sparse distribution of strong defects, and regime III is one to a denser collection of random point disorder [15]. The disorder caused by Ni-substitution at the nanoscale, favors the presence of the SPM. The latter is in agreement with the fact that in systems such as $YBa_2Cu_3O_{7-\delta}$ [48] and $Ba(Fe_{1-x}Co_x)_2As_2$ [14], the SPM is suppressed when the local chemical and electronic uniformity increase by thermal annealing. The regime III with $J_c(H) \approx$ constant can be analyzed in terms of the collective pinning by random point disorder as described by the Larkin-Ovchinnikov theory [49].

The theory of weak collective flux pinning predicts several regimes that depend on the vortex-vortex and vortex–defect interactions. In the SVR, the vortex–vortex interaction is negligible compared to the vortex–defect interaction. When magnetic field is raised, vortex–vortex interactions become dominant, and the vortices are collectively trapped as bundles. The critical current density at the SVR is magnetic field independent expected to follow:

$$J_c \approx J_0 \left(\frac{27 n_d D_v^4}{256 \varepsilon \xi}\right)^{2/3}, \qquad (2)$$

where n_d is point defect density and D_v is the radius of the defects [47]. In the SVR the small-scale displacements of neighboring vortices are independent. The crossover at B^{cr} occurs when the longitudinal displacement correlation length ($L_c^c = \gamma^{-1}\xi(J_0/J_c)^{1/2}$) is larger than the vortex lattice parameter ($a_0 = 1.07(\Phi_0/B)^{1/2}$). For the undoped sample, if we used $J_c^{\text{III regime}}$ (5K) ≈ 0.27 MA cm^{-2}, ξ (0) = 1.4 nm [26], γ ≈ 1 [50] and J_0 ≈ 170 MA cm^{-2}, we theoretically estimate B^{cr} (5 K) ≈ 3.5 T. Although the prediction is qualitatively correct, this value is one order of magnitude smaller than the experimental observations with J_c (H) ≈ constant at high magnetic fields (> 15 T) in ref. [23]. This fact suggests that other sources of pinning contribute to regime III. Indeed, pinning induced by temperature due to planar $CaFe_2As_2$ inclusions do not modify the α exponent, but enhances J_c.

An understanding of the different pinning exhibited by the $CaK(Fe_{1-x}Ni_x)_4As_4$ single crystals is gained from J_c (T) dependences. As we mentioned earlier, undoped crystals display a peak at intermediate temperatures in the J_c (T) dependences when $\mu_0 H$ > 1 T (see Fig. 3*a*). This unusual feature is not present in Ni-doped crystals (see Fig. 3*c*). In addition to the peak at high magnetic fields and temperatures higher than 7 K, the J_c (T/T_c) at $\mu_0 H$ = 0.3 T (mostly regime II) for the undoped crystal is smoother than for the doped ones. On the other hand, the curves at $\mu_0 H$ = 3 T (mostly regime III) show that although J_c increases with temperature, the absolute values below $T_c/2$ for the undoped crystal are systematically smaller than the observed for x up to 0.03. Thus, the unusual peak in J_c (T) at high fields may be related with a weak pinning scenario in which the temperature induces new pinning centers or an increment in the size of the existent ones (see equation 2). However, as we mentioned earlier, it has also been associated with pinning provided by $CaFe_2As_2$ inclusions [16]. The effect is not evidenced in Ni-doped samples because the chemical substitution improves the vortex pinning and masks little changes in the pinning landscape. It is important to note that the J_c (T) values in Fig. 3*a* are approximately 4 times smaller than those reported in ref. [23] for 2.6 μm thick $CaKFe_4As_4$ single crystals, indicating that the vortex pinning is affected by the thickness.

To analyze in more detail the J_c (H, T) dependences, we measured the relaxation of persistent currents as a function of time. Fe-SCs usually display a giant flux creep rate that is well described by the collective pinning theory [32]. The pinning energy depends on the pinning potential and the elastic deformation of the vortices. At low temperatures, the vortices are essentially frozen into their distorted configuration. As the temperature increases, the pinning

strength decreases as a consequence of the thermal fluctuations of the vortex-line. The effective activation energy as a function of current density *J* is given by

$$U_{eff} = \frac{U_0}{\mu}\left[\left(\frac{J_c}{J}\right)^{\mu} - 1\right], \qquad (3)$$

where U_0 is the collective pinning barrier in the absence of a driving force and μ is the regime-dependent glassy exponent [32]. For elastic creep μ > 0 and for plastic creep to μ < 0 [51]. The model of the nucleation of vortex loops predicts for random point defects μ equal to 1/7, 3/2 or 5/2, and 7/9 for single-vortex creep, small-bundle creep, or large-bundle creep, respectively [32]. Using equation 3, the temperature dependence of the creep rate (*S*) results in

$$S = -\frac{\delta ln\, J}{\delta ln\, t} = \frac{T}{U_0 + \mu T ln(\frac{t}{t_0})}, \qquad (4)$$

where *t* is the time and t_0 is an effective hopping attempt time. Equation (4) describes well the presence of a thermally activated Anderson-Kim mechanism at low temperatures ($S \approx T/U_0$) and a plateau in *S* (*T*) in the limit of $U_0 \ll \mu T ln(\frac{t}{t_0})$. Although theoretical models provide a small set of discreet μ values (constant for each regime), experimental studies usually present a gradual evolution of μ from small to large bundles values as *H* is increased [52]. The glassy exponents μ can be obtained from *S* (*T*) data using the extended Maley method [33]. Approximating the current density decays as $\frac{dJ}{dt} = -\left(\frac{J_c}{\tau}\right) e^{-\frac{U_{eff}(J)}{T}}$, the effective activation energy $U_{eff}(J)$ can be experimentally obtained by $U_{eff} = -T\left[ln\left|\frac{dJ}{dt}\right| - C\right]$ (with $C = ln(J_c/\tau)$ a constant factor). To maintain "piecewise" continuity at high *T*, U_{eff} is divided by a thermal factor *G* (*T*) ≤ 1 [53]. In the following the flux creep data and analysis of the glassy exponents will be presented. The summary of μ and U_0 is presented in Table II.

Figure 4*a* shows *S* (*T*) in a $CaKFe_4As_4$ single crystal at $\mu_0 H$ = 0.3 T, 0.5 T, 1 T and 3 T (top x-axis shows the data in T/T_c). Typical curves of *J* (time) are shown in Appendix. The qualitative features of the *S* (*T*) curves are similar to previous observations in Fe-SCs and YBCO single crystals [12,13,14,54]. The main characteristics are the large *S* values (low U_0 values) and modulations in *S* (*T*) (crossovers between vortex regimes). The initial increase of *S* (*T*) corresponds to an Anderson-Kim like creep with $S \approx T/U_0$, except that the nonzero extrapolation

to $S(T=0)$ is usually attributed to a quantum creep component. The quantum creep contribution may be estimated by $S^Q \cong \frac{e^2}{\hbar}\frac{\rho_n}{\xi}\left(\frac{J_c}{J_0}\right)^{1/2}$, where ρ_n is the resistance in the normal state, J_0 is the depairing critical current density, and $\frac{\hbar}{e^2}$ = 4108 Ω [32]. Using ρ_n = 20 μΩ.cm [26], J_0 = 170 MA cm^{-2}, and J_c (0.3 T) ≈ 2 MA cm^{-2} and J_c (3 T) ≈ 0.5 MA cm^{-2}, the S^Q values should be in the range of 0.004-0.002. At intermediate temperatures the flux creep rates depends on the applied magnetic fields. The $S \sim 0.017–0.067$ values are characteristic of collective creep of vortex bundles. The gradual reduction in the S values as the field increases suggest an increment in the glassy exponent μ [52,54]. At temperatures near T_c, the flux creep rates start to be faster as a consequence of change from elastic to plastic relaxation [12]. Figure 4*b* shows the Maley analysis (with $G(T)=1$) for $\mu_o H$ = 0.3 T, 1 T and 3 T. The results show unusual behavior in which U_{eff} (J) displays jump-like discontinuities towards higher U_{eff} values as J decreases. The effect appears both for magnetic fields within regime II and III (see inset Fig. 4*b*). To explain the observed variations it is necessary to consider that U_0 and J_c increase as the temperature rises (see equation 3), indicating the appearance of new pinning centers or a change in the size of the existing ones. This fact is in agreement with the peak in J_c (T) for high magnetic fields discussed above. The U_0 value can be estimated for weak pinning in the SVR by $U_c \approx \frac{H_c^2 \xi^3}{\gamma}\left(\frac{J_c}{J_0}\right)^{1/2}$. An estimate for 10 K in the regime III using ξ (0) = 1.4 nm [26], γ ≈ 1.2 and λ ≈ 200 nm [28], and J_c (10 K) ≈ 0.3 MA.cm^{-2}, yields U_0 ≈ 50 K. As we mentioned earlier, low U_0 values are consistent with the large S values observed even for low temperatures (i. e. S (5 K) ≈ 0.03).

The flux creep relaxation rates S and the Maley analysis for Ni-doped samples are shown in Figures 5 (x= 0.015), 6 (x = 0.025), 7 (x = 0.03) and 8 (x =0.05). Panels (*a*) correspond to $S(T)$ measurements at $\mu_0 H$ = 0.3 T, 1 T and 3 T (top x-axis shows the data in T/T_c). For x = 0.05, due to the shorter extension of the different regimes, the measurements were performed at $\mu_0 H$ = 0.1 T, 0.3 T and 0.5 T. Panels (*b*) and (*c*) display the conventional and extended Maley analysis, respectively. Inset panels (*b*) and (c) show the *H-T* phase diagram indicating the crossovers between vortex regimes and the $G(T)$ function used to maintain “piecewise” continuity, respectively.

The $S(T)$ dependences displayed in the panels (*a*) of Figures 5-8 show features similar to that found for the undoped crystal. The curves usually display a peak at the temperature where there

is a crossover from regimes II to III. Moreover, the curves at different fields shift to smaller *S* values. For example, S (T_c/2,) at 3 T is 0.026 for x = 0.015, 0.022 for **x** = 0.025 and 0.018 for x = 0.03. The changes in the *S* values with temperature and fields may be related to changes in the glassy exponent μ. In systems such as $YBa_2Cu_3O_7$ its value evolves from ≈ 1/7 (theoretical prediction for SRV) to ≈ 3/2 at maximum of the SPM (theoretical prediction for small bundles) [52,54].

The extended Maley analysis of data displayed in panels (*b*) of Figures 5-8 is shown in panels (*c*). Like the undoped crystal, U_0 in the regime III changes with temperature. For instance, U (J) for x = 0.015 at $\mu_o H$ = 3 T shows jump discontinuities towards higher U_{eff} as J decreases (see Fig. 5*b*). Moreover, for 1 T at T > 12 K (regime III), the piecewise continuity is maintained with an unusual in G (T) (see inset Fig. 5*c*). Furthermore, the G (T) dependences used to maintain piecewise continuity at $\mu_o H$ = 3 T in x = 0.025 and x = 0.03 are different to the used at smaller fields. We analyze the glassy exponent μ and U_0 at the regime II using equation 3. For x = 0.015, 0.025 and 0.03 the analysis was performed at $\mu_o H$ = 0.3 T and 1 T, and for x = 0.05 at $\mu_o H$ = 0.1 T and 0.3 T. The results are summarized in Table II. The fits are indicated in the panels (*c*) of Figures 5-8. The μ value for 0.3 T evolves from 0.55 to 0.97 when x increases from 0.015 to 0.05. Moreover for 1 T, it increases from 0.64 to 1.25 when x increases from 0.015 to 0.03. The evolution of the μ (x) at the same field may be related to different scales in H/H_{c2} and a gradual crossover from values predicted for SVR (1/7) and small bundles (3/2) [52,54], indicating similar pinning mechanisms over the whole range of compositions. There are no particular features that can be related to the coexistence of superconductivity and AFM. The influence of T_c and related parameters such as H_{c2} in the μ (x) dependence is clearly evidence for $\mu^{0.3\ T}$ = 0.55 (0.03) in x =0.015 (with T_c = 31 K) and $\mu^{0.1\ T}$ = 0.54 (0.03) in x = 0.05 (with T_c =10.1 K). The low U_0 values (typically < 100 K) contribute to the large *S* values displayed for all the samples over the whole range of temperature. Moreover, we observed that U_0 decreases as field increases, indicating that the changes in the absolute S values with magnetic fields at low temperatures are mainly related to changes in μ (see eq. 4). For the undoped crystals, due to the similarity in the S (T) dependences, the glassy exponents μ and the U_0 are expected to be of the same order than in Ni-doped samples. The main differences may be related to both of the small coherence length ξ and of the absence of extended pinning centers. Slight modifications in the pinning landscape of the undoped crystals improve the pinning as is evidenced in the peak at the J_c (T) dependences. Small Ni addition increases the disorder masking small variations in the pinning landscape with temperature. Nevertheless, the Maley analysis indicates

that U_0 at regime III also changes for the doped samples. Considering that planar $CaFe_2As_2$ intergrowths are over the entire range of chemical compositions [16], their contribution to the vortex pinning is stronger for undoped crystals.

Finally, it is important to mention that, as is evidenced from Figures 2*a* and 2*b*, the J_c values in the undoped crystals may be significantly enhanced by adding pinning centers. One of the most effective methods to improve pinning in superconductors with short ξ is particle irradiation [4]. Depending on the mass and energy of the ions and for adequate dose, U_0 in Fe-SCs may increases from tens of Kelvins to 300 – 500 K [4,14]. The J_c^{sf} (5 K) ≈ 1.7 - 2 MA.cm^{-2} in $CaKFe_4As_4$ is similar that value found in single crystals of $YBa_2Cu_3O_{7-d}$ (≈ 2 MA cm^{-2} [55]) and $Ba_{0.6}K_{0.4}Fe_2As_2$ (≈ 2 MA cm^{-2} [56]). Moreover, the value duplicates the typically observed in optimal doped $Ba(Fe,Co)_2As_2$ [14]. As was previously noticed, $CaKFe_4As_4$ single crystals display high anisotropy in the pinning properties due to planar defects [16,17,23]. The presence of $CaFe_2As_2$ intergrowths improves considerably the J_c for **H** // *ab* [16,17]. Furthermore, the comparison with previously reported data in thinner single crystals suggests that the pinning mechanisms are strongly affected by thickness [23].

4. Conclusions

We have performed magnetic measurements on single crystals of $CaK(Fe_{1-x}Ni_x)_4As_4$ (x ≈ 0, 0.015, 0.025, 0.03 and 0.05). The J_c (H) dependences usually display a power-law regime followed by a SPM. The magnetic relaxation of all the crystals is well described by the collective creep theory. The samples display glassy exponent μ within the predictions for vortex bundles in a weak pinning scenario and relatively small characteristic pinning energy (U_0 < 100 K). Comparatively, the undoped crystals display low J_c values at high magnetic fields and low temperatures. Small Ni doping improves the vortex pinning and enhances the J_c in the whole range of magnetic fields. The self-field J_c shows a discontinuous break to smaller values as the samples develop an AFM ordered ground state that coexists with a competing superconducting state. Moreover, the magnetic field dependences of J_c at intermediate values are more gradual as Ni doping increases. These changes are smoother for x > 0.015, suggesting that AFM domains affect the vortex pinning. The undoped crystal displays an unusual peak in J_c (T) at high fields. The enhancement in J_c (T) matches with an unexpected increase in U_0 and the

appearance of a SPM. Ni doping induces a SPM in the $J_c(H)$ dependences for the whole range of temperature. The analysis of the vortex dynamics for small and intermediate magnetic fields shows a gradual evolution in the glassy exponent μ with Ni-content, x. This implies that there is no appreciable change in the mechanism that determines the vortex relaxation for Ni-doped samples with and without magnetic order. The large J_c values observed in the undoped crystal, even for low chemical disorder, suggest that they can be significantly enhanced adding pinning centers.

Acknowledgments

This work was supported by the U.S. Department of Energy, Office of Basic Energy Science, Division of Materials Sciences and Engineering. The research was performed at the Ames Laboratory. Ames Laboratory is operated for the U.S. Department of Energy by Iowa State University under Contract No. DE-AC02-07CH11358. WRM was supported by the Gordon and Betty Moore Foundation's EPiQS Initiative through Grant GBMF4411. NH is partially supported by ANCYP PICT2015-2171 (Argentina).

Appendix

The critical current densities J_c were estimated from the Bean model using the appropriate geometrical factor in the Bean Model [35,36]. Figure 9 shows the hysteresis loops under **H**||*c* in Ni-doped $CaK(Fe_{1-x}Ni_x)_4As_4$ single crystals at several temperatures. The curves are obtained for magnetic fields between $\mu_0 H$ = - 1 T and $\mu_0 H$ = 5 T. For each temperature before starting the measurements, an initial negative magnetic field $H \sim 4\ H^*$ is applied (to guarantee the critical state at the first point).

The flux creep rates were obtained as $S = -{}^{\delta lnJ}/_{\delta lnt}$ from the time dependence of the magnetization at different fields and temperature. Figure 10 shows typical curves of J (time) for a $CaKFe_4As_4$ single crystal.

List of Tables

List of Figures

phase diagram with the $J_c(H)$ regimes indicated in Fig. 2*b*. *c*) Extended Maley for $\mu_o H$ = 0.3 T and 1 T from curves displayed in panel *b)*.Fits using equation 3 are indicated .Inset shows the $G(T)$ function used to normalize U_0. The data is obtained using C = 13.

Figure 6. *a*) Creep rate (S) vs. temperature (bottom x-axis) and reduced temperature T/T_c (top x-axis) at different applied magnetic fields for a $CaK(Fe_{0.975}Ni_{0.025})_4As_4$ single crystal. *b)* Maley analysis with $\mu_o H$ = 0.3 T, 1 T and 3 T. The data is obtained with $G(T)$ = 1. Inset shows an *H-T* phase diagram with the $J_c(H)$ regimes indicated in Fig. 2c. *c*) Extended Maley for $\mu_o H$ = 0.3 T and 1 T from curves displayed in panel *b)*.Fits using equation 3 are indicated .Inset shows the $G(T)$ function used to normalize U_0. The data is obtained using C = 13.

Figure 7. *a*) Creep rate (S) vs. temperature (bottom x-axis) and reduced temperature T/T_c (top x-axis) at different applied magnetic fields for a $CaK(Fe_{0.97}Ni_{0.03})_4As_4$ single crystal. *b)* Maley analysis with $\mu_o H$ = 0.3 T, 1 T and 3 T. The data is obtained with $G(T)$ = 1. Inset shows an *H-T* phase diagram with the $J_c(H)$ regimes indicated in Fig. 2c. *c*) Extended Maley for $\mu_o H$ = 0.3 T and 1 T from curves displayed in panel *b)*.Fits using equation 3 are indicated .Inset shows the $G(T)$ function used to normalize U_0. The data is obtained using C = 13.

Figure 8. *a*) Creep rate (S) vs. temperature (bottom x-axis) and reduced temperature T/T_c (top x-axis) at different applied magnetic fields for a $CaK(Fe_{0.95}Ni_{0.05})_4As_4$ single crystal. *b)* Maley analysis with $\mu_o H$ = 0.1 T, 0.3 T and 0.5 T. The data is obtained with $G(T)$ = 1. Inset shows an *H-T* phase diagram with the $J_c(H)$ regimes indicated in Fig. 2*e*. *c*) Extended Maley for the curves displayed in panel *b)*. Fits using equation 3 are indicated. Inset shows the $G(T)$ function used to normalize U_0. The data is obtained using C = 13.

Figure 9. *a-e)* Magnetization loops with **H**||*c* in Ni-doped $CaK(Fe_{1-x}Ni_x)_4As_4$ (x = 0, x = 0.015, x = 0.025, x = 0.03 and x = 0.05) single crystals at several temperatures. The curves correspond to magnetic fields between $\mu_0 H$ = -1 T and 5 T.

Figure 10. Current density J as a function of time (logarithmic scales) for T = 5 K, 7 K, 8 K and 10 K for a $CaKFe_4As_4$ single crystal with $\mu_0 H$ = 0.3 T applied **H**||*c*.

Table I.

Sample	T_c (K)	$J_c^{sf}(5\ K)$ (MA cm^{-2})	α	Thickness (μm)
$CaKFe_4As_4$	35.0	1.7	0.68	34
$CaKFe_4As_4$	35.0	2.0	0.68	14
$CaK(Fe_{0.985}Ni_{0.015})_4As_4$	31.1	2.8	0.56	25
$CaK(Fe_{0.975}Ni_{0.025})_4As_4$	25.0	1.7	0.47	37
$CaK(Fe_{0.97}Ni_{0.03})_4As_4$	20.5	1.3	0.46	58
$CaK(Fe_{0.95}Ni_{0.05})_4As_4$	10.1	0.1	0.40	38

Table II.

$CaK(Fe_{1-x}Ni_x)_4As_4$	0.015			0.025			0.03			0.05		
	μ	U_0	J_c	μ	U_0	J_c	μ	U_0	J_c	μ	U_0	J_c
0.1 T	-	-	-	-	-	-	-	-	-	0.54*	60	0.42
0.3 T	0.55*	90	5.0	0.62*	110	3.3	0.69*	95	2.2	0.97#	38	0.33
1 T	0.64*	55	4.2	1.04*	70	2.2	1.25*	45	1.8	-	-	-

Figure 1.

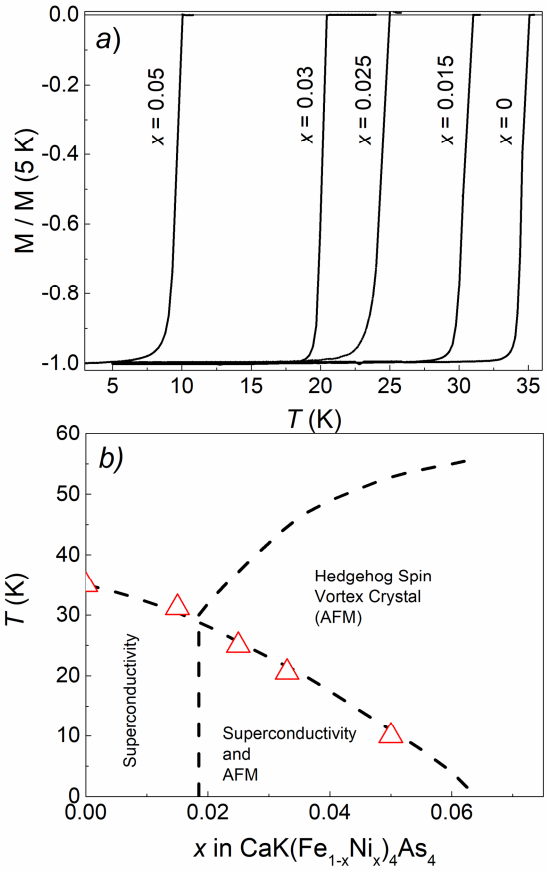
a)
x = 0.05
x = 0.03
x = 0.025
x = 0.015
x = 0
M / M (5 K)
T (K)
b)
Hedgehog Spin
Vortex Crystal
(AFM)
Superconductivity
Superconductivity
and
AFM
T (K)
x in CaK(Fe1-xNix)4As4

Figure 2.

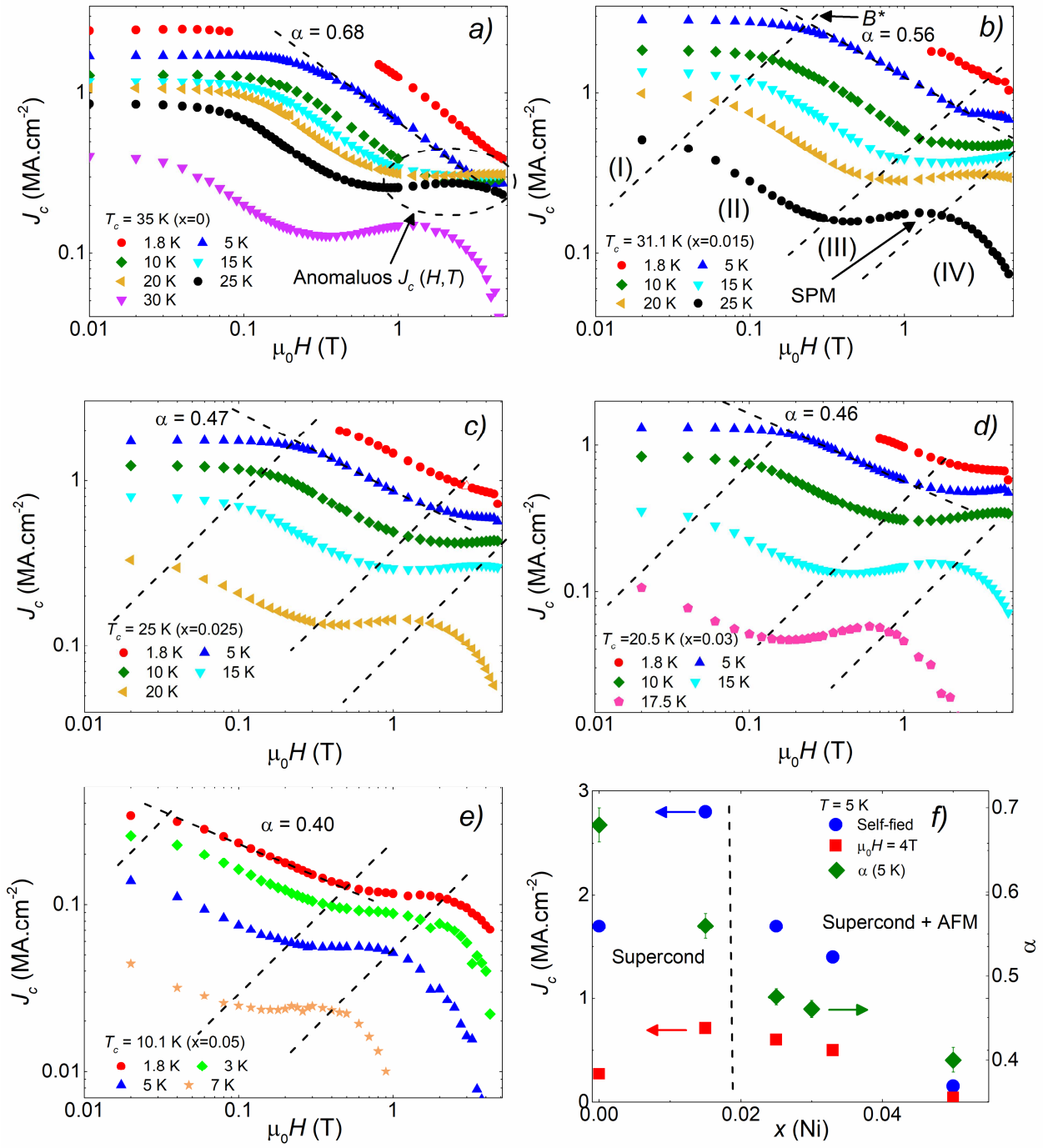
a)
α = 0.68
T_c = 35 K (x=0)
1.8 K
5 K
10 K
15 K
20 K
25 K
30 K
Anomaluos J_c (H,T)
J_c (MA.cm^{-2})
$\mu_0 H$ (T)
b)
B*
α = 0.56
(I)
(II)
(III)
(IV)
SPM
T_c = 31.1 K (x=0.015)
c)
α = 0.47
T_c = 25 K (x=0.025)
d)
α = 0.46
T_c =20.5 K (x=0.03)
17.5 K
e)
α = 0.40
T_c = 10.1 K (x=0.05)
3 K
7 K
f)
T = 5 K
Self-fied
$\mu_0 H$ = 4T
α (5 K)
Supercond
Supercond + AFM
x (Ni)
α

Figure 3

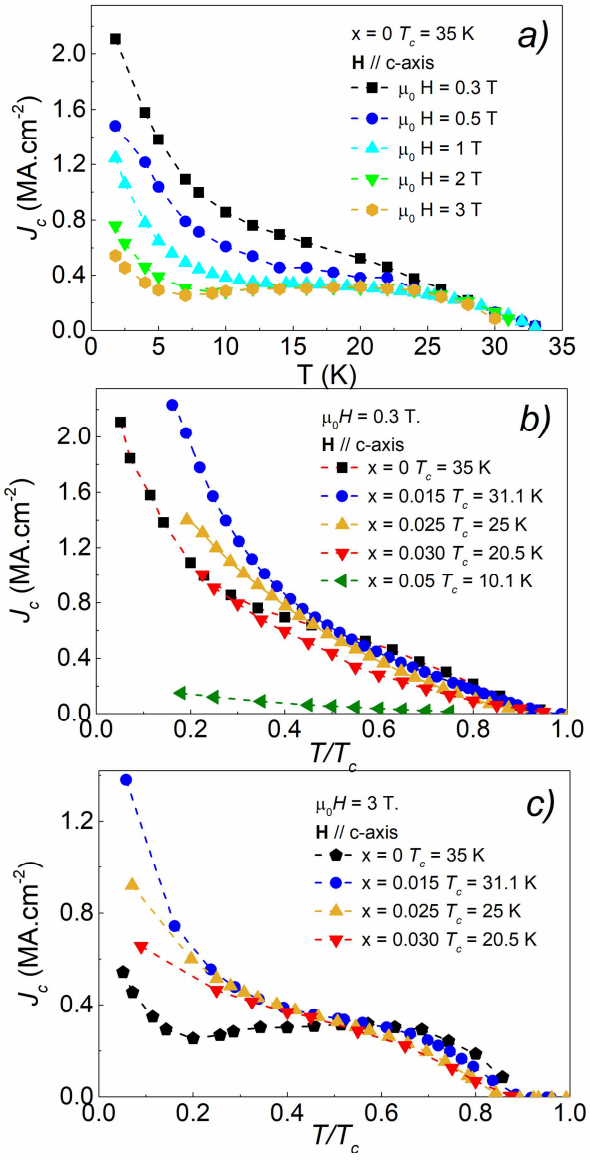
a)
x = 0 T_c = 35 K
H // c-axis
μ_0 H = 0.3 T
μ_0 H = 0.5 T
μ_0 H = 1 T
μ_0 H = 2 T
μ_0 H = 3 T
J_c (MA.cm^{-2})
T (K)
b)
$\mu_0 H$ = 0.3 T.
H // c-axis
x = 0 T_c = 35 K
x = 0.015 T_c = 31.1 K
x = 0.025 T_c = 25 K
x = 0.030 T_c = 20.5 K
x = 0.05 T_c = 10.1 K
J_c (MA.cm^{-2})
T/T_c
c)
$\mu_0 H$ = 3 T.
H // c-axis
x = 0 T_c = 35 K
x = 0.015 T_c = 31.1 K
x = 0.025 T_c = 25 K
x = 0.030 T_c = 20.5 K
J_c (MA.cm^{-2})
T/T_c

Figure 4.

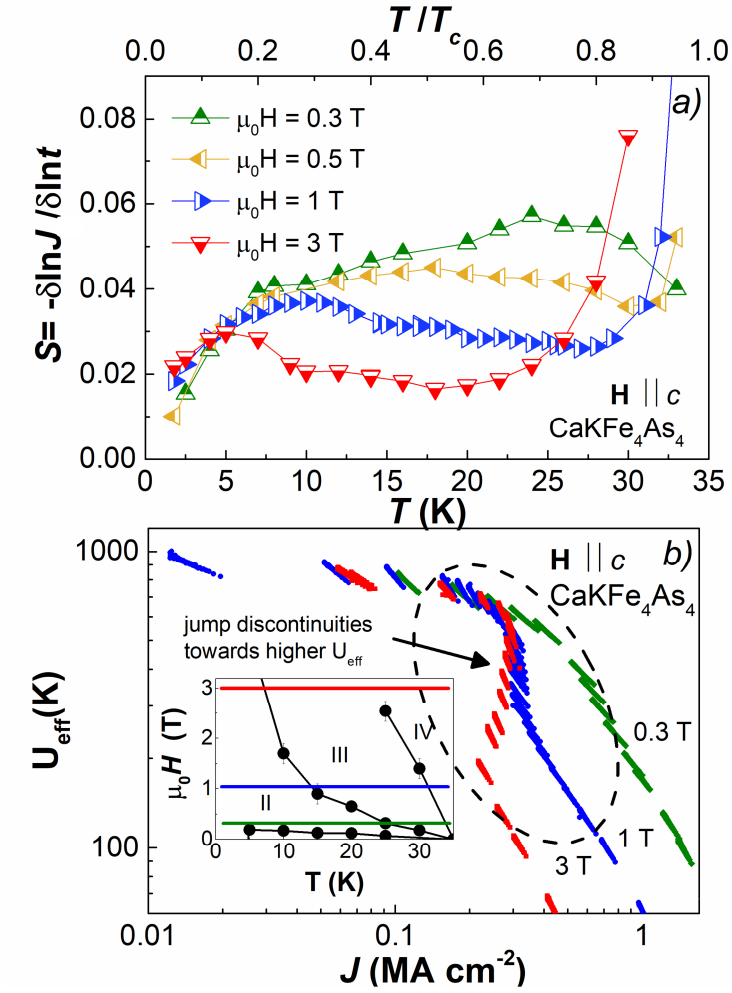
T /T_c
0.0
0.2
0.4
0.6
0.8
1.0
a)
μ0H = 0.3 T
μ0H = 0.5 T
μ0H = 1 T
μ0H = 3 T
H || c
CaKFe4As4
S= -δlnJ /δlnt
0.00
0.02
0.04
0.06
0.08
0
5
10
15
20
25
30
35
T (K)
b)
H || c
CaKFe4As4
jump discontinuities
towards higher Ueff
0.3 T
1 T
3 T
Ueff(K)
1000
100
μ0H (T)
T (K)
II
III
IV
0.01
0.1
1
J (MA cm-2)

Figure 5.

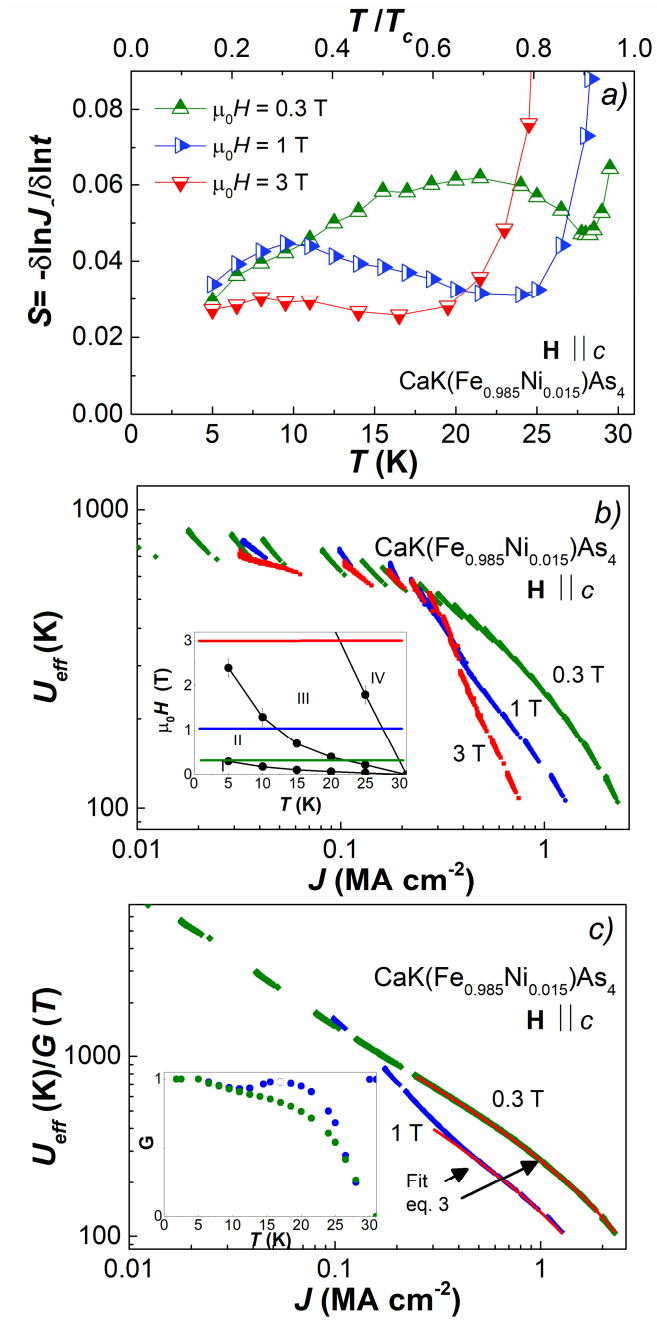
T /T_c
0.0
0.2
0.4
0.6
0.8
1.0
a)
μ0H = 0.3 T
μ0H = 1 T
μ0H = 3 T
H || c
CaK(Fe0.985Ni0.015)As4
S= -δlnJc/δlnt
T (K)
b)
CaK(Fe0.985Ni0.015)As4
H || c
0.3 T
1 T
3 T
μ0H (T)
II
III
IV
T (K)
Ueff (K)
J (MA cm-2)
c)
CaK(Fe0.985Ni0.015)As4
H || c
0.3 T
1 T
Fit
eq. 3
G
T (K)
Ueff (K)/G (T)
J (MA cm-2)

Figure 6.

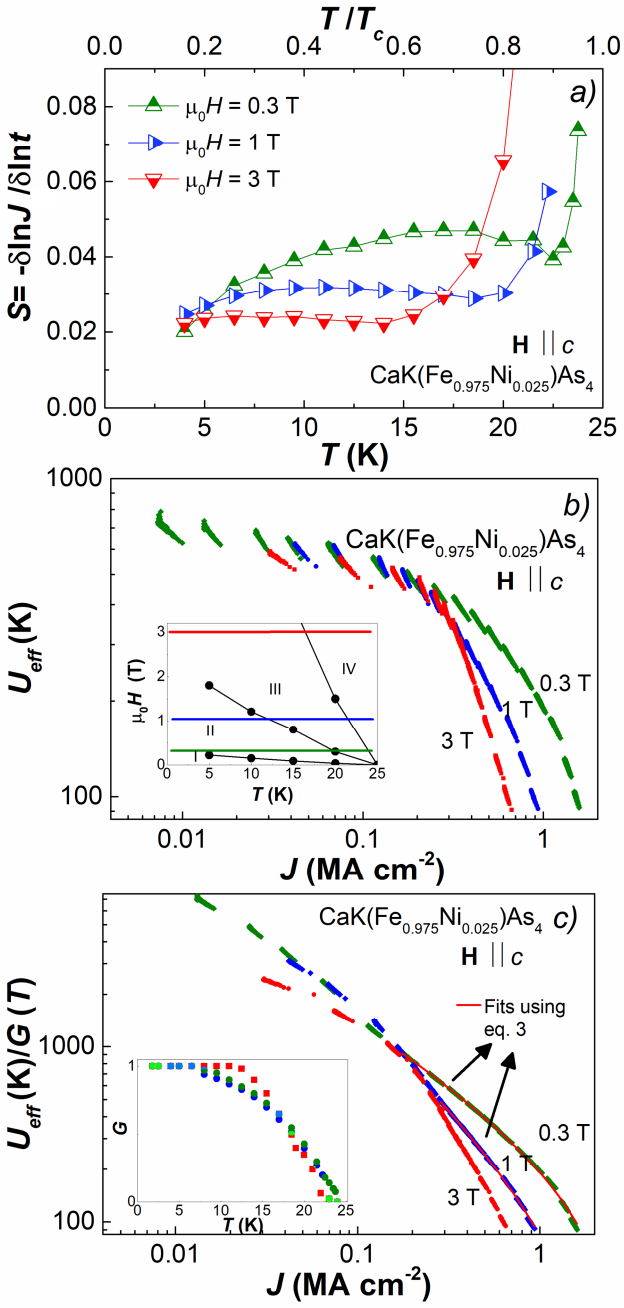
T /T_c
0.0
0.2
0.4
0.6
0.8
1.0
a)
μ0H = 0.3 T
μ0H = 1 T
μ0H = 3 T
S= -δlnJ /δlnt
H || c
CaK(Fe0.975Ni0.025)As4
T (K)
b)
CaK(Fe0.975Ni0.025)As4
H || c
0.3 T
1 T
3 T
μ0H (T)
I
II
III
IV
T (K)
Ueff (K)
J (MA cm-2)
c)
CaK(Fe0.975Ni0.025)As4
H || c
Fits using eq. 3
0.3 T
1 T
3 T
G
T (K)
Ueff (K)/G (T)
J (MA cm-2)

Figure 7.

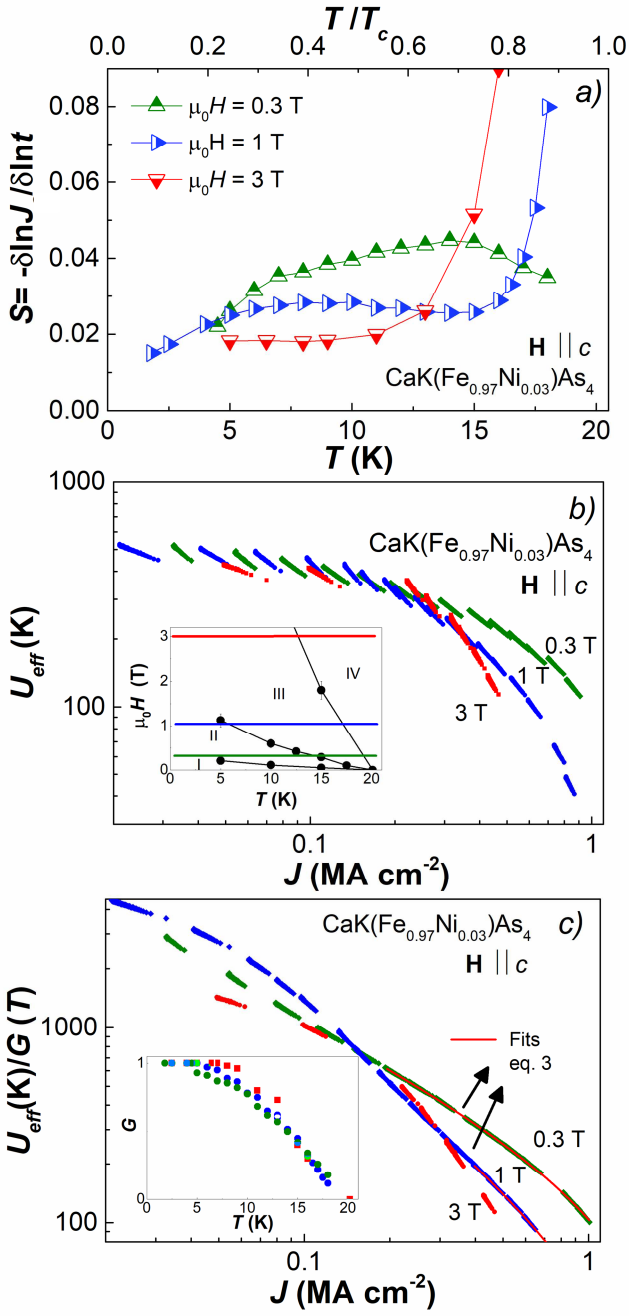
T /T_c
0.0
0.2
0.4
0.6
0.8
1.0
a)
μ0H = 0.3 T
μ0H = 1 T
μ0H = 3 T
S= -δlnJ /δlnt
0.00
0.02
0.04
0.06
0.08
H || c
CaK(Fe0.97Ni0.03)As4
0
5
10
15
20
T (K)
b)
CaK(Fe0.97Ni0.03)As4
H || c
0.3 T
1 T
3 T
Ueff (K)
1000
100
μ0H (T)
I
II
III
IV
T (K)
0.1
1
J (MA cm-2)
c)
CaK(Fe0.97Ni0.03)As4
H || c
Fits
eq. 3
0.3 T
1 T
3 T
Ueff(K)/G (T)
1000
100
G
T (K)
0.1
1
J (MA cm-2)

Figure 8.

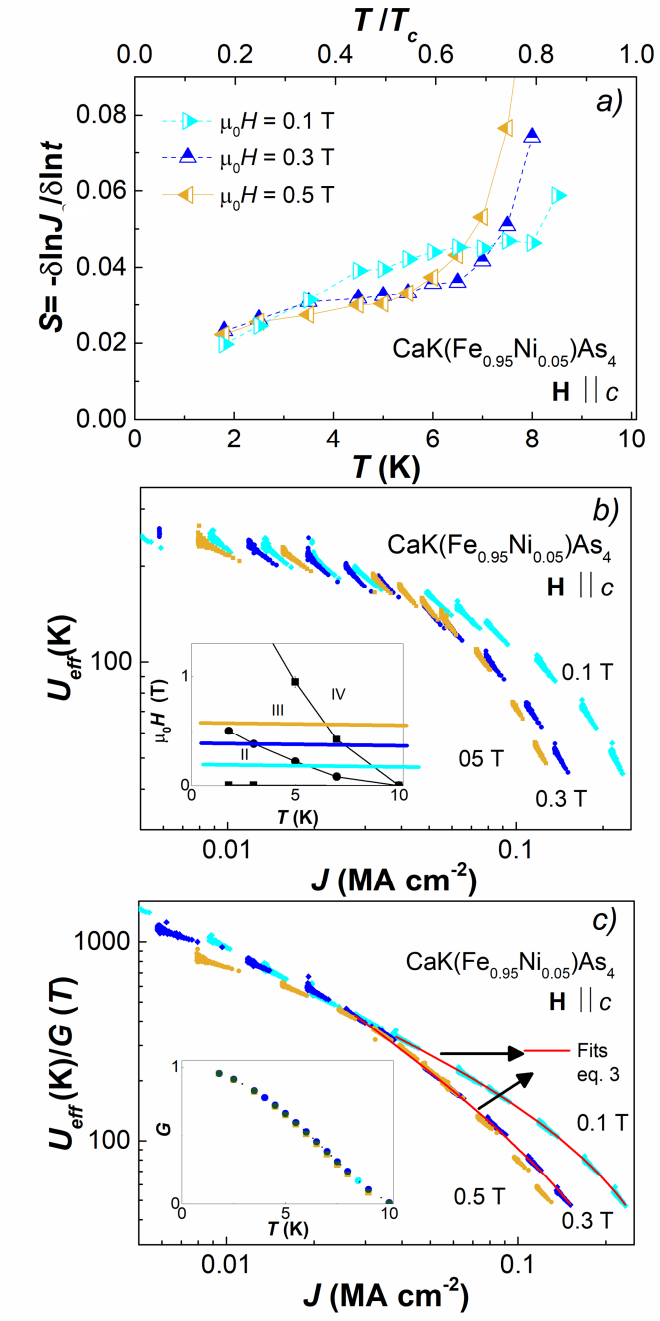
T /T_c
0.0
0.2
0.4
0.6
0.8
1.0
a)
μ0H = 0.1 T
μ0H = 0.3 T
μ0H = 0.5 T
S= -δlnJ /δlnt
0.08
0.06
0.04
0.02
0.00
CaK(Fe0.95Ni0.05)As4
H || c
0
2
4
6
8
10
T (K)
b)
CaK(Fe0.95Ni0.05)As4
H || c
Ueff (K)
100
0.1 T
05 T
0.3 T
μ0H (T)
1
0
III
IV
II
0
5
10
T (K)
0.01
0.1
J (MA cm-2)
c)
CaK(Fe0.95Ni0.05)As4
H || c
Ueff (K)/G (T)
1000
100
Fits
eq. 3
0.1 T
0.5 T
0.3 T
G
1
0
0
5
10
T (K)
0.01
0.1
J (MA cm-2)

Figure 9.

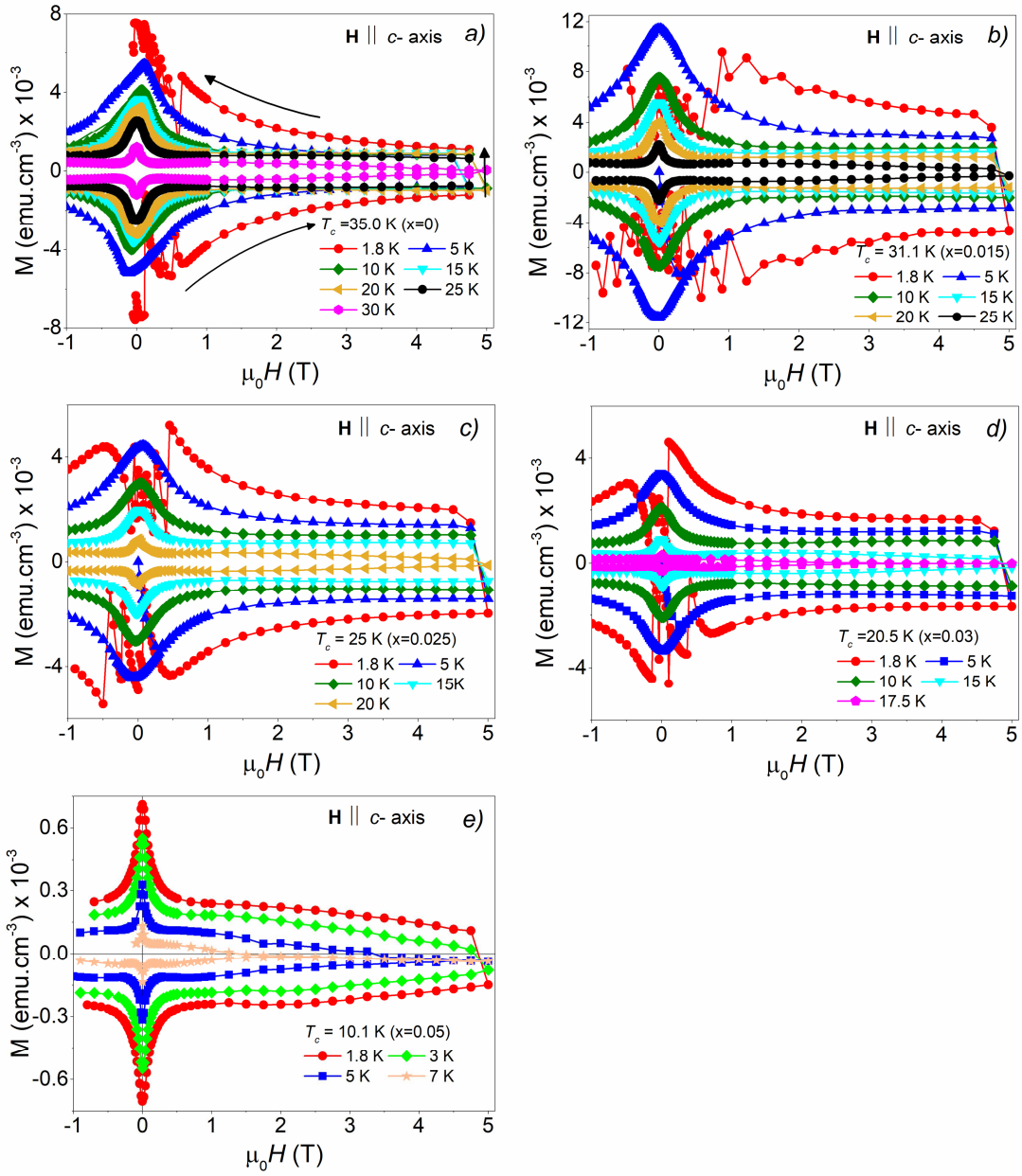
H || c- axis
a)
M (emu.cm-3) x 10-3
μ0H (T)
Tc =35.0 K (x=0)
1.8 K
5 K
10 K
15 K
20 K
25 K
30 K
H || c- axis
b)
M (emu.cm-3) x 10-3
μ0H (T)
Tc = 31.1 K (x=0.015)
1.8 K
5 K
10 K
15 K
20 K
25 K
H || c- axis
c)
M (emu.cm-3) x 10-3
μ0H (T)
Tc = 25 K (x=0.025)
1.8 K
5 K
10 K
15K
20 K
H || c- axis
d)
M (emu.cm-3) x 10-3
μ0H (T)
Tc =20.5 K (x=0.03)
1.8 K
5 K
10 K
15 K
17.5 K
H || c- axis
e)
M (emu.cm-3) x 10-3
μ0H (T)
Tc = 10.1 K (x=0.05)
1.8 K
3 K
5 K
7 K

Figure 10.

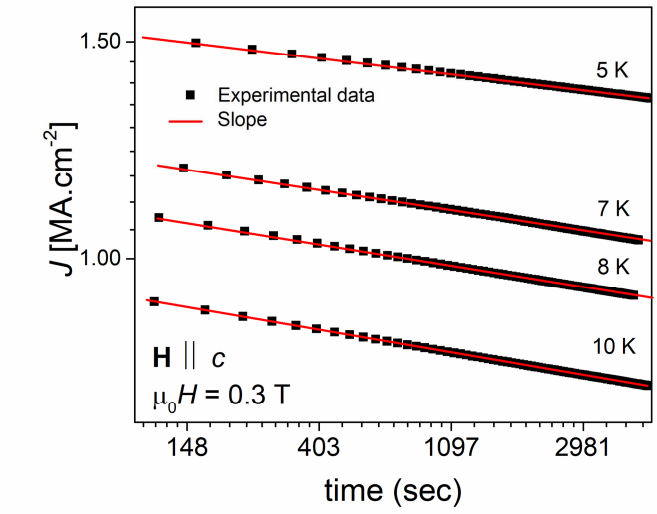

[1] Roland Willa, Alexei E. Koshelev, Ivan A. Sadovskyy, and Andreas Glatz, Phys. Rev. B **98**, 054517 (2018).
[2] H. Hosono, A. Yamamoto, H. Hiramatsu, and Y. Ma, Mater. Today 21, 278 (2018).
[3] L. Fang, Y. Jia, J. A. Schlueter, A. Kayani, Z. L. Xiao, H. Claus, U. Welp, A. E. Koshelev, G. W. Crabtree, and W.-K. Kwok. Phys. Rev B **84**, 140504(R) (2011).
[4] Wai-Kwong Kwok, Ulrich Welp, Andreas Glatz, Alexei E. Koshelev, Karen J. Kihlstrom , and George W Crabtree. Rep. Prog. Phys. **79,** 116501 (2016).
[5] I. I. Mazin. Nature (London) **464**, 183 (2010).
[6] Xianhui Chen, Pengcheng Dai, Donglai Feng, Tao Xiang, and Fu-Chun Zhang. National Science Review **1**, 371 (2014).
[7] Kazutaka Kudo, Keita Iba, Masaya Takasuga, Yutaka Kitahama, Jun-ichi Matsumura, Masataka Danura, Yoshio Nogami, and Minoru Nohara. Scientific Reports **3**, 1478 (2013).
[8] A. Chubukov, and P. J. Hirschfeld. Physics Today **68**, 46 (2015).
[9] H. Okabe, N. Takeshita, K. Horigane, T. Muranaka, and J. Akimitsu. Phys. Rev B **81**, 205119 (2010).
[10] S. K. Kim, M. S. Torikachvili, E. Colombier, A. Thaler, S. L. Bud'ko, and P. C. Canfield. Phys. Rev B **84,** 134525 (2011).
[11] Sergey L. Bud'ko, Yong Liu, Thomas A. Lograsso, and Paul C. Canfield. Phys. Rev. B **86**, 224514 (2012).
[12] R. Prozorov, N. Ni, M. A. Tanatar, V. G. Kogan, R. T. Gordon, C. Martin, E. C. Blomberg, P. Prommapan, J. Q. Yan, S. L. Bud'ko, and P. C. Canfield. Phys. Rev. B 78, 224506 (2008).
[13] Y. Nakajima, Y. Tsuchiya, T. Taen, T. Tamegai, S. Okayasu, and M. Sasase, Phys. Rev. B **80**, 12510 (2009).

[14] N. Haberkorn, Jeehoon Kim, K. Gofryk, F. Ronning, A. S. Sefat, L. Fang, U. Welp, W. K. Kwok, and L. Civale. Supercond. Sci. Technol. **28**, 055011 (2015).
[15] C. J. van der Beek, G. Rizza, M. Konczykowski, P. Fertey, I. Monnet, Thierry Klein, R. Okazaki, M. Ishikado, H. Kito, A. Iyo, H. Eisaki, S. Shamoto, M. E. Tillman, S. L. Bud'ko, P. C. Canfield, T. Shibauchi, and Y. Matsuda. Phys. Rev B **81**, 174517 (2010).
[16] Shigeyuki Ishida, Akira Iyo, Hiraku Ogino, Hiroshi Eisaki, Nao Takeshita, Kenji Kawashima, Keiichi Yanagisawa, Yuuga Kobayashi, Koji Kimoto, Hideki Abe, Motoharu Imai, Jun-ichi Shimoyama & Michael Eisterer npj Quantum Materials 4, 27 (2019).
[17] Sunseng Pyon, Ayumu Takahashi, Ivan Veshchunov, Tsuyoshi Tamegai, Shigeyuki Ishida, Akira Iyo, Hiroshi Eisaki, Motoharu Imai, Hideki Abe, Taichi Terashima, and Ataru Ichinose. Phys. Rev B **99**, 104506 (2019).
[18] C.-L. Song, Yi-Lin Wang, Ye-Ping Jiang, Lili Wang, Ke He, Xi Chen, Jennifer E. Hoffman, Xu-Cun Ma, and Qi-Kun Xue. Phys. Rev. Lett. **109**, 137004 (2012).
[19] Wen-He Jiao, Qian Tao, Zhi Ren, Yi Liu, and Guang-Han Cao. npj Quantum Materials **2,** 50 (2017).
[20] Vasily S. Stolyarov, Ivan S. Veshchunov, Sergey Yu. Grebenchuk, Denis S. Baranov, Igor A. Golovchanskiy, Andrey G. Shishkin, Nan Zhou, Zhixiang Shi, Xiaofeng Xu, Sunseng Pyon, Yue Sun, Wenhe Jiao, Guang-Han Cao, Lev Ya. Vinnikov, Alexander A. Golubov, Tsuyoshi Tamegai, Alexander I. Buzdin, and Dimitri Roditchev. Sci. Adv. **4**, 1061 (2018).
[21] Sergey L. Bud'ko, Vladimir G. Kogan, Ruslan Prozorov, William R. Meier, Mingyu Xu, and Paul C. Canfield. Phys. Rev B **98**, 144520 (2018).
[22] Wang Cheng, Hai Lin, Bing Shen, and Hai-Hu Wen. Science Bulletin **64**, 81 (2019).
[23] Shiv J. Singh, Matthew Bristow, William R. Meier, Patrick Taylor, Stephen J. Blundell, Paul C. Canfield, and Amalia I. Coldea. Phys. Rev Mater **2**, 074802 (2018).
[24] A. Iyo, K. Kawashima, T. Kinjo, T. Nishio, S. Ishida, H. Fujihisa, Y. Gotoh, K. Kihou, H. Eisaki, and Y. Yoshida, J. Am. Chem. Soc. **138**, 3410 (2016).
[25] Daixiang Mou, Tai Kong, William R. Meier, Felix Lochner, Lin-Lin Wang, Qisheng Lin, Yun Wu, S. L. Bud'ko, Ilya Eremin, D. D. Johnson, P. C. Canfield, and Adam Kaminski. Phys. Rev Lett **117**, 277001 (2016).
[26] W. R. Meier, T. Kong, U. S. Kaluarachchi, V. Taufour, N. H. Jo, G. Drachuck, A. E. Bohmer, S. M. Saunders, A. Sapkota, A. Kreyssig, M. A. Tanatar, R. Prozorov, A. I. Goldman, Fedor F. Balakirev, Alex Gurevich, S. L. Bud'ko, and P. C. Canfield. Phys. Rev B **94**, 064501 (2016).
[27] Udhara S. Kaluarachchi, Valentin Taufour, Aashish Sapkota, Vladislav Borisov, Tai Kong, William R. Meier, Karunakar Kothapalli, Benjamin G. Ueland, Andreas Kreyssig, Roser Valentí, Robert J. McQueeney, Alan I. Goldman, Sergey L. Bud'ko, and Paul C. Canfield. Phys. Rev B **96**, 140501(R) (2017).
[28] Rustem Khasanov, William R. Meier, Yun Wu, Daixiang Mou, Sergey L. Bud'ko, Ilya Eremin, Hubertus Luetkens, Adam Kaminski, Paul C. Canfield, and Alex Amato. Phys. Rev B **97**, 140503(R) (2018).
[29] Antón Fente, William R. Meier, Tai Kong, Vladimir G. Kogan, Sergey L. Bud'ko, Paul C. Canfield, Isabel Guillamón, and Hermann Suderow. Phys Rev B **97**, 134501 (2018).

[30] W. R. Meier, Q.-P. Ding, A. Kreyssig, S. L. Bud'ko, A. Sapkota, K. Kothapalli, V. Borisov, R. Valentí, C. D. Batista, P. P. Orth, R. M. Fernandes, A. I. Goldman, Y. Furukawa, A. E. Böhmer, and P. C. Canfield, Npj Quantum Mater. **3**, 5 (2018).

[31] A. Kreyssig, J. M. Wilde, A. E. Böhmer, W. Tian, W. R. Meier, Bing Li, B. G. Ueland, Mingyu Xu, S. L. Bud'ko, P. C. Canfield, R. J. McQueeney, and A. I. Goldman. Phys. Rev. B **97**, 224521 (2018).

[32] G. Blatter, M. V. Feigel'man, V. B. Geshkenbein, A. I. Larkin, and V. M. Vinokur, Rev. Mod. Phys. **66**, 1125 (1994).

[33] M. P. Maley, J. O. Willis, H. Lessure, M. E. McHenry. Phys. Rev. B **42,** 2639 (1990).

[34] W. R. Meier, T Kong, T., S. L. Bud'ko, P. C. Canfield, Phys. Rev. Mater. **1**, 013401 (2017).

[35] C. P. Bean, Phys. Rev. Lett. **8**, 250 (1962); C. P. Bean, Rev. Mod. Phys. 36, 31 (1964).

[36] E. M.Gyorgy, R. B. Van Dover, K. A. Jackson, L. F. Schneemeyer, J. V. Waszczak, Appl. Phys. Lett. **55**, 283 (1989).

[37] Y. Yeshurun, A. P. Malozemoff, A. Shaulov, Rev. Mod. Phys. **68**, 911(1996).

[38] F. Ohtake, T. Taen, S. Pyon, T. Tamegai, S. Okayasu, T. Kambara, and H. Kitamura, Physica C 518, 47 (2015).

[39] N. Haberkorn, B. Maiorov, I. O. Usov, M. Weigand, W. Hirata, S. Miyasaka, S. Tajima, N. Chikumoto, K. Tanabe, and Leonardo Civale. Phys. Rev. B **85,** 014522 (2012).

[40] R. Prozorov, M. A. Tanatar, N. Ni, A. Kreyssig, S. Nandi, S. L. Bud'ko, A. I. Goldman, and P. C. Canfield, Phys. Rev. B 80, 174517 (2009).

[41] Bing Shen, Peng Cheng, Zhaosheng Wang, Lei Fang, Cong Ren, Lei Shan, and Hai-Hu Wen. Phys. Rev B 81, 014503 (2010).

[42] Dongjoon Song, Shigeyuki Ishida, Akira Iyo, Masamichi Nakajima, Jun-ichi Shimoyama, Michael Eisterer and Hiroshi Eisaki, Scientific Reports **6,** 26671 (2016).

[43] S. Salem-Sugui Jr., L. Ghivelder, A. D. Alvarenga, L. F. Cohen, K. A. Yates, K. Morrison, J. L. Pimentel, Jr., Huiqian Luo, Zhaosheng Wang, and Hai-Hu Wen, Phys. Rev. B **82**, 054513 (2010).

[44] F. Hengstbergera, M. Eisterer, and H. W. Weber, Appl. Phys. Lett. **96**, 022508 (2010).

[45] N. Haberkorn, M. Miura, B. Maiorov, G. F. Chen, W. Yu, and L. Civale. Phys. Rev. B **84**, 094522 (2011).

[46] N. Haberkorn, Jeehoon Kim, S. Suárez, Jae-Hun Lee, and S. H. Moon, Supercond. Sci. Technol. 28, 125007 (2015).

[47] C. J. van der Beek, M. Konczykowski, A. Abal'oshev, I. Abal'osheva, P. Gierlowski, S. J. Lewandowski, M. V. Indenbom, and S. Barbanera, Phys. Rev. B **66**, 024523 (2002).

[48] A. Oka, S. Koyama, T. Izumi, Y. Shiohara, J. Shibata and T. Hirayama. Japan. J. Appl. Phys. **39,** 5822 (2000).

[49] A. I. Larkin and Yu. N. Ovchinnikov, J. Low Temp. Phys. **34**, 409 (1979).

[50] H. Q. Yuan, J. Singleton, F. F. Balakirev, S. A. Baily, G. F. Chen, J. L. Luo, and N. L. Wang. Nature (London) **457**, 565 (2009).

[51] Y. Abulafia, A. Shaulov, Y. Wolfus, R. Prozorov, L. Burlachkov, Y. Yeshurun, D. Majer, E. Zeldov, H. Wühl, V. B. Geshkenbein, and V. M. Vinokur, Phys. Rev. Lett. 77, 1596 (1996).

[52] J. R. Thompson, Y. R. Sun, D. K. Christen, L. Civale, A. D. Marwick, and F. Holtzberg. Phys. Rev. B **49**, 13287(R) (1994).

[53] J. G. Ossandon, J. R. Thompson, D. K. Christen, B. C. Sales, Yangren Sun, and K. W. Lay. Phys. Rev. B **46**, 3050 (1992).
[54] L. Civale, L. Krusin-Elbaum, J. R. Thompson and F. Holtzberg. Phys. Rev. B **50,** 7188 (1994).
[55] L. Civale, A. D. Marwick, T. K. Worthington, M. A. Kirk, J. R. Thompson, L. Krusin-Elbaum, Y. Sun, J. R. Clem, and F. Holtzberg. Phys. Rev Lett **67**, 648 (1991).
[56] L. Fang, Y. Jia, C. Chaparro, G. Sheet, H. Claus, M. A. Kirk, A. E. Koshelev, U. Welp, G. W. Crabtree, W. K. Kwok, S. Zhu, H. F. Hu, J. M. Zuo, H.-H. Wen, and B. Shen. Appl. Phys. Lett **101**, 012601 (2012).